processes

MDPI

Article

Characterization and Comparison of Anammox Immobilization in Polyvinyl Alcohol, Polyethylene Glycol and Water-Borne Polyurethane

Yi Yang [1,2], Hui Gong [2], Zhen Zhou [1] and Xiaohu Dai [2,*]

[1] School of Environmental and Chemical Engineering, Shanghai Electric Power University, Shanghai 200090, China
[2] College of Environmental Science and Engineering, Tongji University, Shanghai 200092, China
* Correspondence: daixiaohu@tongji.edu.cn

Abstract: Anammox bacteria were embedded with different mass fractions of polyvinyl alcohol (PVA), polyethylene glycol (PEG) and water-based polyurethane (WPU) materials. The embedded immobilized pellets with different particle sizes of about 2.8–3.2 mm were prepared. The effects of the mass fraction of the embedding material (PVA 6–12%, PEG 6–9%, WPU 10%) and the concentration of activated carbon added in the embedding process (0–4%) on the pellet was investigated. The performance of pellet formation, sedimentation rate, mechanical strength, expansion coefficient, and elasticity were compared and analyzed under different immobilization conditions, and the parameters of each embedding step were optimized. Anammox immobilized pellets prepared with 10% polyvinyl alcohol (PVA), 2% sodium alginate (SA), and 2% powdered activated carbon were proposed. The effects of salinity on anammox were investigated through a batch test, and the optimal reaction conditions were selected to carry out the operation test. The functional groups of embedded and unembedded anammox sludge were detected using the infrared spectrum. A continuous flow sequencing batch reactor (SBR) demonstrated stable operation with immobilized anammox. Scanning electron microscopy revealed that the immobilized anammox pellets appeared as irregular particles, with each micro-unit predominantly being spherical. Additionally, a minor presence of rod-shaped bacteria was also noted. After 30 days of stable operation of the reactor, the ammonia nitrogen removal rate reached 84.7%.

Keywords: anammox; immobilization; polyvinyl alcohol; polyethylene glycol; polyurethane

Citation: Yang, Y.; Gong, H.; Zhou, Z.; Dai, X. Characterization and Comparison of Anammox Immobilization in Polyvinyl Alcohol, Polyethylene Glycol and Water-Borne Polyurethane. *Processes* **2024**, *12*, 1442. https://doi.org/10.3390/pr12071442

Academic Editor: Qunshan Wei

Received: 8 June 2024
Revised: 28 June 2024
Accepted: 2 July 2024
Published: 10 July 2024

1. Introduction

Anaerobic ammonia oxidation (anammox) represents a straightforward and cost-effective method for nitrogen removal in wastewater treatment [1]. Its growing application in managing high-ammonia nitrogen wastewaters marks it as a promising technology in this field. Anammox converts ammonia and nitrite nitrogen to nitrogen gas without requiring oxygen or a carbon source, with a minor byproduct of nitrate nitrogen [2]. This process, known for its energy efficiency, is operational in over 120 wastewater treatment plants for sludge reject water [3]. Anammox sludge is a complex microbial community that thrives under high cell concentrations, making the maintenance of high concentrations and minimal losses in reactors a key challenge for its application [4].

In recent years, immobilized microorganism technology has emerged as a significant research area with promising applications in wastewater treatment. The embedding method, which entraps microbial cells or enzymes in a polymer or membrane matrix, is the most extensively studied and applied immobilization technique [5,6]. The principle of embedding [7] is that microbial cells or enzymes are trapped in the polymer to form a network space with many pores, in which the matrix can permeate and diffuse [8]. This method not only shields microbial cells [9] from ammonia nitrogen load and pollutants

but also provides ample space for their growth and reproduction, thereby retaining high biomass levels [10]. The embedding process can be categorized into various techniques, including gel [11], microcapsule, and fiber embedding [12].

The integration of microbial embedding technology with anammox to create immobilized pellets is expected to enhance the process's stability [13]. For instance, Xu utilized polyvinyl alcohol to embed immobilized activated sludge, demonstrating effective ammonia nitrogen removal even under high-ammonia nitrogen conditions [5]. Similarly, Chen initiated an anammox reactor using embedded anammox bacteria particles and water-borne polyurethane, achieving stable operation within 49 days with notable nitrogen removal rates over 80.7% [10].

Embedding–immobilization technology is effective in preventing the loss of anammox sludge, maintaining biomass concentration and activity in reactors, and enhancing treatment capacity, indicating significant potential for application [14]. However, research on embedded anammox sludge is limited, and particles produced using current embedding materials often exhibit inadequate mechanical strength, reduced biological activity, and instability over extended operations. Commonly used immobilizing agents like polyvinyl alcohol (PVA) [15], polyethylene glycol (PEG) [16], and polyacrylamide [17] are favored for their non-toxicity, elasticity, toughness, and biocompatibility in water treatment. PVA, a water-soluble polymer [18], is primarily used as a binder and dispersant. It stands out for its water solubility, biodegradability, and non-toxicity. PVA hydrogels are noted for their high water absorption [19], significant swelling in water [20], and excellent mechanical properties. PEG, a colorless polyether polymer, is soluble in various solvents due to its strong polarity, enabling it to form hydrophilic hydrogen bonds [21]. Its amphipathy, biocompatibility, and reactivity at its molecular ends, coupled with a wide range of molecular weights, offer versatility in scaffold preparation. By adjusting the molecular weight and dosage ratio, PEG can create alginate scaffolds with tailored porosity, suitable for sustained-release applications [22]. Polyethylene glycol is a typical pore-making agent, which can increase the porosity and surface area of gel. Sodium alginate (SA), as a natural polysaccharide, can form hydrogels under relatively mild conditions to avoid the inactivation of active substances. In combination with sodium alginate (SA), PVA can enhance the mechanical strength and surface characteristics of particles. The addition of activated carbon improves particle agglomeration, while curing agents contribute to a stable internal network structure [23]. Water-borne polyurethane (WPU) is another material with excellent biocompatibility and mechanical properties, capable of forming stable hydrogels [24]. The main components of polyurethane, including polyether polyols [25], polyester polyols [26], and isocyanates [27], determine its physical properties. Polyurethane's multifunctionality [28] allows it to be tailored for various applications through adjustments in material composition and preparation [29]. Adding activated carbon to the embedding material can accelerate the mass transfer of the substrate in the embedding pellet and improve its mass transfer performance. Because activated carbon has a large specific surface area, the porosity of the embedded carrier is further improved, the microbial capacity of the embedded carrier is also improved, and more anammox bacteria are enriched. Because the density of powdered activated carbon is much less than the density of water, if the amount of activated carbon is too much, the density of embedded pellets is greatly reduced, and it can not settle and suspend well in artificial wastewater. The effect of wastewater treatment is affected. Therefore, the concentration of activated carbon added is controlled within a certain range.

This study utilizes polyvinyl alcohol, polyethylene glycol, and water-borne polyurethane for embedding anammox sludge, adding powdered activated carbon to enhance the mechanical strength and mass transfer performance of the pellets. This approach aims to reduce expansion coefficients, improve mass transfer performance, and accelerate anammox bacteria enrichment, thereby significantly enhancing treatment efficiency. This study also measures properties like sedimentation velocity, mechanical strength, swelling, and elasticity to assess the performance of these embedded particles [30]. The optimal em-

bedding method was selected to explore the influencing factors in the anammox process, and the optimal reaction conditions were selected to operate the anammox reactor, which ultimately provided strong support for the application of anammox technology [31].

2. Materials and Methods

2.1. Preparation of Immobilized Particles

The anammox sludge used for embedding and immobilization was sourced from a large-scale reactor in the Changsha pilot project, which operated continuously and stably. Initially, the sludge underwent a triple washing process with deionized water and phosphate-buffered saline (PBS) to eliminate residual substrates from its surface. The embedding and immobilization procedures were as follows: (1) A blend of polyvinyl alcohol (PVA) solution and 2% sodium alginate (SA) solution was uniformly mixed. This mixture was then combined with an equal volume of acclimated centrifugal anammox sludge. Subsequently, a calculated amount of powdered activated carbon (AC) was added. The blend was then dropped into a mixture of 1% $CaCl_2$ and saturated with H_3BO_3 using a syringe. After cross-linking in a 4 °C refrigerator for 12 h, the mixture was discarded, and the pellets were rinsed with distilled water for 30 s. They were then placed in 100 mL of 0.5 mol/L KH_2PO_4 solution for phosphorylation for one hour. The final embedded particles were obtained after sifting and a final rinse with distilled water. (2) A specific concentration of polyethylene glycol (PEG) solution and 2% SA solution were mixed uniformly and combined with an equal volume of acclimated centrifugal anammox sludge. A measured amount of powdered AC was then added. The mixture was dripped into a combination of 1% $CaCl_2$ and saturated H_3BO_3 using a syringe. Following cross-linking at 4 °C for 12 h, the mixture was discarded, and the pellets were rinsed with distilled water for 30 s before being placed in 100 mL of 0.5 mol/L KH_2PO_4 solution for phosphorylation for one hour. The final embedded particles were acquired after sifting and a final rinse. (3) WPU embedded particles: The WPU solution with a mass fraction of 10% was mixed with the acclimated anammox sludge after equal volume centrifugation. Then, according to the mass percentage [32], powdered activated carbon with a certain mass fraction, 0.24% N, N-methylene bisacrylamide and 1.5% potassium persulfate were added, and the mixture was quickly stirred to a solid gel after about 30 min.

2.2. Physicochemical Characterization of Embedded Pellets and Particles

2.2.1. Measurement of Sedimentation Rate

The actual sedimentation rate was determined by injecting a 100 mL cylinder with water and leveling the liquid to the 100 mL mark. Timing commenced when a ball was introduced into the cylinder and ended when it reached the bottom. The formula for calculating the actual sedimentation rate was u = L (the height of the cylinder's water level) divided by t (time). Multiple measurements were averaged for accuracy. The theoretical sedimentation rate was calculated using the formula for the free sedimentation velocity of spherical solid particles in a Newtonian liquid (Formula (1)):

$$u = (\rho_s - \rho)gd^2/18\mu \quad (1)$$

where u is the sedimentation rate of spherical solid particles (cm/s), ρ_s is the spherical solid particle density (g/cm^3), ρ is the density of water (g/cm^3), d is the spherical solid particle diameter (cm), and μ is the viscosity of water for 1.14×10^{-3} Pa·s.

2.2.2. Measurement of Mechanical Strength

To assess the mechanical properties of the embedded pellets, 100 uniformly sized pellets were placed in a 300 mL conical flask. Distilled water was added to reach the 300 mL mark, and the flask was subjected to magnetic stirring at 600 rpm for 48 h. Following this

duration, the extent of damage to the embedded pellets was observed to evaluate their mechanical strength. The mechanical strength (M) was calculated using Equation (2):

$$M = N'/N \quad (2)$$

where N′ is the number of intact embedded particles remaining after stirring, and N is the initial number of embedded particles.

The gel particles prepared by the water-based polyurethane embedding material in this study are standard cubes of 3 × 3 × 3 mm, and their force area can be accurately measured. When the sample particles are broken, the maximum pressure value that can be borne is the strength value of the particles. Before the test, the sample was soaked in water at room temperature and stored. During the test, the surface water was dried with filter paper. The average value was measured 10 times each time, and the mechanical strength was calculated according to Equation (3):

$$P = F_{max}/S \quad (3)$$

where P (kg/m^2) is particle strength, F_{max} (kg) is the maximum pressure the gel particle can withstand, and S (m^2) is the force area of the gel particle.

2.2.3. Measurement of the Expansion Coefficient

To evaluate the expansion coefficient of the embedded pellets, 100 uniformly sized pellets were placed in a 300 mL conical flask. Deionized water was added to bring the volume to 300 mL, and the flask was gently agitated at 30 °C for 48 h. The diameter of each pellet was measured before and after the oscillation period using a vernier caliper. The expansion coefficient (E) was calculated using Equation (4):

$$E = D'/D \quad (4)$$

where D′ is the average diameter of the embedded particles after oscillation, and D is the average diameter of the embedded particles before oscillation.

2.2.4. The Elasticity Is Measured as Follows

To assess the elasticity of the embedded balls, three well-formed and uniformly sized specimens were arranged on a slide, which was then covered with a cover slip. The initial height (H_0) between the two slides was measured. Subsequently, a 50 g weight was added to the cover slip, and the new height (H_1) between the slides was recorded. The ratio H_1/H_0 was used to evaluate the elasticity, with a smaller ratio indicating better elasticity. The evaluation scale was as follows: "✔✔✔" for the best elasticity, "✔" for the worst, and "✔✔" for intermediate elasticity.

2.2.5. Determination of Mass Transfer Coefficient

To elucidate the impact of the material carrier on the internal diffusion behavior and cell characteristics, the mass transfer coefficient was experimentally determined for ammonium (NH_4^+-N) in immobilized anammox pellets. To minimize uncertainty, the pellets were aerated in pure water for 20 min prior to testing to eliminate residual ammonia nitrogen. The experimental setup involved placing the anammox embedded pellets in a 250 mL conical flask and adding 150 mL of simulated wastewater with the composition detailed in Table 1. The volume ratio of pellets to wastewater was 1:4. The mixture was then shaken at 34 °C and 120 rpm in a constant-temperature shaker [33]. Samples were collected at 0, 10, 30, 60, and 90 min to measure the NH_4^+-N concentration. To maintain consistency, the sampling volume was controlled to be less than 1% of the total solution volume to mitigate the impact of sampling on wastewater concentration.

Table 1. Composition of the manual simulation wastewater.

Components	Concentration	Components	Concentration
NH_4Cl	50 mgN/L	$NaNO_2$	65 mgN/L
KH_2PO_4	5 mg/L	$CaCl_2$	0.5 g/L
trace element I	1 mL/L	trace element II	1 mL/L

The mass transfer coefficient of embedded pellets can be calculated according to Equation (5):

$$-\ln \frac{C_t - C_\infty}{C_0 - C_\infty} \cong \frac{\pi^2 D_e}{R^2} t - \ln \frac{6}{\pi^2} \quad (5)$$

In Equation (5), D_e is the effective mass transfer coefficient, mm^2/h; C_0 is the initial concentration of NH_4^+-N, mg/L; C_∞ is the final NH_4^+-N concentration, mg/L; C_t is the concentration of NH_4^+-N at the time of sampling, mg/L; R is the small spherical radius of gel embedding, mm; t is the sampling time, h. It can be seen from the above formula that D_e is a function of $\ln(C_t - C_\infty)/(C_0 - C_\infty)$ and R and t; then, the slope $k = \pi^2 D_e/R^2$ is plotted with time t as the abscissa and $-\mathrm{In}(C_t - C_\infty)/(C_0 - C_\infty)$ as the ordinate, and the effective mass transfer coefficient is calculated as $D_e = k \times R^2/\Pi^2$.

2.3. Microbial Activity Batch Test under Various Salinity Levels

Following a cultivation period at 34 °C and the successful activation of the embedded pellets, a series of batch tests were conducted to investigate the effects of various factors on the anammox reaction process. The experiments were performed in 1 L conical flasks with a pellet dosing rate of 15%. Samples were collected every 2 h to evaluate the denitrification performance of the anammox embedding balls over a 12 h period within the flasks. To examine the impact of salinity on the nitrogen removal efficiency of the embedded pellet by anammox, specific operating parameters were controlled throughout the experimentation, including NH_4^+-N concentration, NO_2^--N concentration, temperature, pH, and dissolved oxygen. The only variable manipulated was the influent NaCl concentration, which was incrementally increased. The influent NH_4^+-N concentration was 100 mg/L, with an influent NO_2^--N concentration of 120 mg/L, a temperature of 34 °C, a pH range of 7.4–7.5, and a reaction period of 12 h. The nitrogen removal performance of the anammox embedded pellets was assessed at NaCl concentrations of 5 g/L, 10 g/L, and 15 g/L in the influent.

2.4. Operation of the Reactor Filled with Immobilized Anammox Pellets

The reactor, constructed from plexiglass, possesses an effective volume of 0.5 L and is equipped with a stirring mechanism, a manual water inlet, and outlet systems. The experimental setup utilized artificial simulated wastewater, with NH_4^+-N provided by ammonium chloride and NO_2^--N sourced from sodium nitrite, maintaining a ratio of 1:1.2. The concentration of the nutrients was adjusted according to the anaerobic anammox reaction process. The composition of the artificial wastewater is detailed in Table 2. In the reactor, the pellet dosage rate was set at 20%, with the influent NH_4^+-N concentration at 100 mg/L and the NO_2^--N concentration at 120 mg/L. The temperature was maintained at 34 °C, the pH was regulated to 7.4–7.5, and the hydraulic retention time (HRT) was set at 6 h. Four groups of reactors were established. The first reactor, R_1, contained non-embedded anammox sludge at a concentration of 4.05 g-VSS L^{-1}. Subsequently, R_2, R_3, and R_4 were inoculated with embedded anammox sludge pellets, each at a different sludge concentration of 1.25 g-VSS L^{-1}, 2.84 g-VSS L^{-1}, and 3.78 g-VSS L^{-1}, respectively. The stable operational load of the reactors was evaluated through a comparative analysis.

Table 2. Anammox manual simulation of wastewater composition.

Component	Concentration, mg/L	Component	Concentration, mg/L
NH_4Cl	on-demand configuration	KH_2PO_4	10
$NaNO_2$	on-demand configuration	$KHCO_3$	1250
$CaCl_2 \cdot 2H_2O$	3.6	trace element I	1 mL/L
$MgSO_4 \cdot 7H_2O$	300	trace element II	1 mL/L

2.5. Morphological Observation of Immobilized Anammox Pellets by Scanning Electron Microscope

On the 10th day of reactor operation, a selection of representative anammox sludge pellets was retrieved for analysis. These samples were meticulously cleaned by rinsing them three times with 0.1 mol/L phosphate buffer. Following this, the samples underwent fixation at 5 °C for 12 h using a 2.5% glutaraldehyde solution. Subsequently, the pellets were dehydrated through a graded ethanol series, culminating in 100% ethanol. Finally, the dehydrated samples were dried using a critical point dryer (K850, Quorum Technologies LTD, Lewes, UK). The dried sample was then split in half to facilitate the observation of its cross-sectional structure. After coating with gold, the surface morphology of the embedded pellets was meticulously examined using a scanning electron microscope (Nippon Electronics, JSM-IT300, Tokyo, Japan).

3. Results and Discussion

3.1. Comparison of Immobilized Anammox Pellets of PVA, PEG, and WPU

3.1.1. Determination and Analysis of Sedimentation Rate

The choice of polyvinyl alcohol (PVA) mass fraction significantly affects the ease of forming embedding pellets. When the PVA mass fraction is 4%, the resulting pellets are challenging to form, often yielding a mass of embedded bacteria rather than discrete pellets. At a PVA mass fraction of 5%, the pellets readily adhere to each other upon addition of a cross-linker. However, when the PVA mass fraction exceeds 12%, the resulting gel solution becomes excessively viscous, forming cylindrical shapes that are difficult to drop. Consequently, the PVA mass fraction was determined to be 6%, 8%, 10%, and 12% to optimize pellet formation. To ensure the efficacy of PEG-based embedding pellets, the mass fraction of PEG was selected as 6%, 7%, 8%, and 9% following several experimental iterations to further investigate their physical and chemical properties. The molecular weight distribution of hydrogel WPU was studied, and it was determined that gel reaction occurred in 10%WPU solution. Therefore, 10%WPU solution was selected to prepare particles, and an appropriate amount of powdered activated carbon was added to improve its mechanical strength and mass transfer performance.

As depicted in Figure 1, the theoretical sedimentation rate demonstrates a trend of increasing with the mass fraction of the embedding material. In Figure 1a, the pellet embedded with 10% polyvinyl alcohol (PVA) by mass fraction exhibits the highest actual settling rate. This is attributed to the pellet's favorable forming effect, well-defined shape, substantial actual density, and a settling rate of 3.6 cm/s, which signifies its superior settling performance. Consequently, the pellets embedded with 10% PVA were chosen for further investigation.

In Figure 1b, the pellet embedded with 9% polyethylene glycol (PEG) by mass fraction has the highest settling rate, although this is accompanied by a relatively large error. The pellet embedded with 8% PEG by mass fraction closely matches the settling rate of the 9% PEG pellet and demonstrates good settling performance. Therefore, the pellet embedded with 8% PEG by mass fraction was selected for subsequent exploration.

In Figure 1c, the sedimentation rates of particles embedded in a 10% water-based polyurethane (WPU) solution with 1%, 2%, 3%, and 4% powdered activated carbon are shown. The incorporation of activated carbon enhances porosity, surface area, and microbial capacity within the pellets. Initially, as the mass fraction of activated carbon increases, the

actual sedimentation rate also increases before eventually decreasing. The pellet with 3% powdered activated carbon exhibits the highest sedimentation rate of 3.35 cm/s.

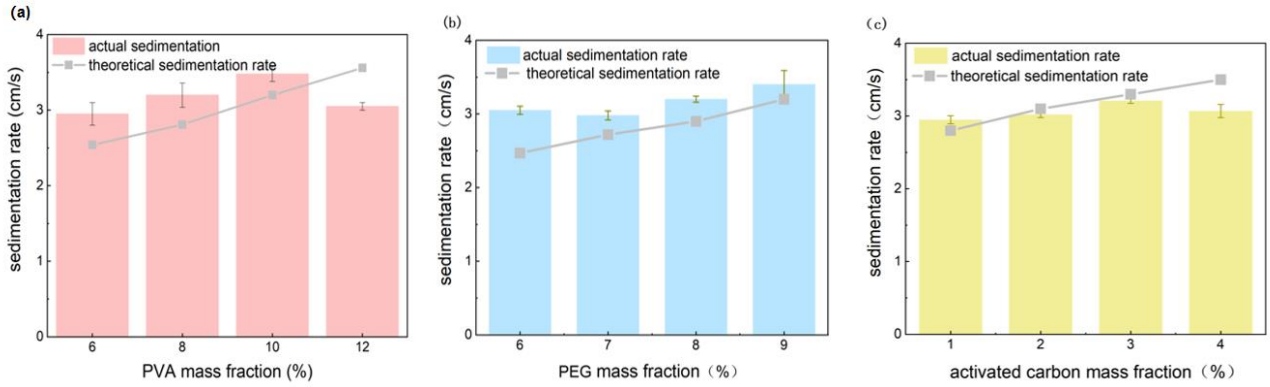

Figure 1. Sedimentation rate of embedded materials with different mass fractions: (**a**) PVA; (**b**) PEG; (**c**) WPU.

3.1.2. Mechanical Strength Analysis

In the 10% polyvinyl alcohol–sodium alginate (PVA-SA) embedded beads, the mechanical strength was measured after adding 1%, 2%, 3%, and 4% powdered activated carbon. The results are presented in Figure 2a. After 24 h of magnetic stirring, the beads with 1% and 3% activated carbon showed slight erosion and turbidity in the solution, indicating the breakdown of the embedding balls. However, the beads with 2% and 4% activated carbon maintained their integrity, with strengths of 97.7% and 98%, respectively. After 36 h, the difference in mechanical strength between the beads with 1%, 2%, 3%, and 4% activated carbon was more pronounced, with the 2% activated carbon beads achieving a strength of 97.5%. By 48 h, the damage rate of the beads with 1% activated carbon approached 5%, while the beads with 3% and 4% activated carbon also became turbid. Surprisingly, the beads with 2% activated carbon remained clear and demonstrated a mechanical strength close to 97%. These findings indicate that the addition of activated carbon significantly enhances the mechanical strength of the beads, with the optimal concentration being 2%.

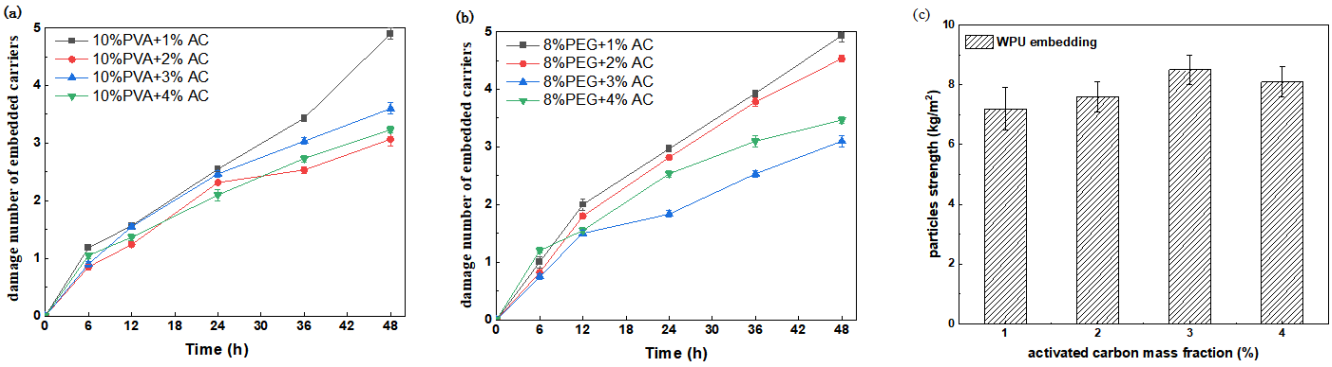

Figure 2. Mechanical strength of embedded pellets and particles with different embedding materials added to powdered activated carbon: (**a**) PVA; (**b**) PEG; (**c**) WPU.

In the 8% polyethylene glycol–sodium alginate (PEG-SA) embedded beads, the mechanical strength was evaluated following the addition of 1%, 2%, 3%, and 4% powdered activated carbon. The results are depicted in Figure 2b. After 12 h of magnetic stirring, the damage rate of the beads with 1% and 2% activated carbon was higher than those with 3% and 4% activated carbon. The beads with 3% and 4% activated carbon exhibited a mechanical strength of 98.5%. After 24 h, the solution with 1% and 2% activated carbon was cloudy, and the beads' surfaces showed slight erosion. The damage rates of the beads with 3% and 4% activated carbon were notably different, with mechanical strengths of

98.2% and 97.5%, respectively. The beads with 3% activated carbon displayed the best mechanical stability. By 36 h, the damage rate of the beads with 1%, 2%, and 4% activated carbon exceeded that of the beads with 3% activated carbon. After 48 h, the beads with 3% activated carbon maintained the lowest damage rate compared to the initial state and approached a mechanical strength of 97%.

In this study, the maximum pressure that the gel particles can withstand is determined to be the strength of the particles. WPU can be polymerized catalytically to form stable hydrogels. Hydrogels are a type of polymer characterized by their three-dimensional network structure, which can achieve a significant relative molecular mass. This network is formed through cross-linked chemical bonds such as hydrogen bonds. Adding different mass fractions of powdered activated carbon influences the strength of gel particles, the experimental results of which are shown in Figure 2c. The mechanical strength of water-based polyurethane gel particles first increased and then decreased with the increase in activated carbon addition, and the optimal strength was reached when the mass fraction of activated carbon was 3%. The rationale behind this choice lies in the fact that a modest quantity of activated carbon can adsorb water within the gel, thereby bolstering its mechanical robustness. However, an excessive amount of activated carbon may disrupt the gel's mesh structure, leading to a decline in particle strength. Consequently, gel particles containing 3% activated carbon are selected for further examination.

3.1.3. The Coefficient of Expansion Is Measured and Analyzed

The expansion coefficient is a critical physical and chemical parameter for embedded immobilized beads and particles. An excessive expansion coefficient can result in microbial leakage due to the gel's water absorption and swelling. In the case of PVA-SA embedded beads, adding varying concentrations of powdered activated carbon (1%, 2%, 3%, and 4%) was assessed. As shown in Figure 3a, after 6 h of shaking, the expansion rates were 112%, 112.7%, 117%, and 119% for the respective carbon concentrations. This order of expansibility (4%AC > 3%AC > 2%AC > 1%AC) suggests that the addition of activated carbon enhances the porosity, specific surface area, and permeability of the pellets, which is beneficial for microbial activity. After 48 h of shaking, the swelling ability of the 2% and 4% activated carbon carriers was similar. Given the cost implications in wastewater treatment applications, the 2% activated carbon was selected for further study.

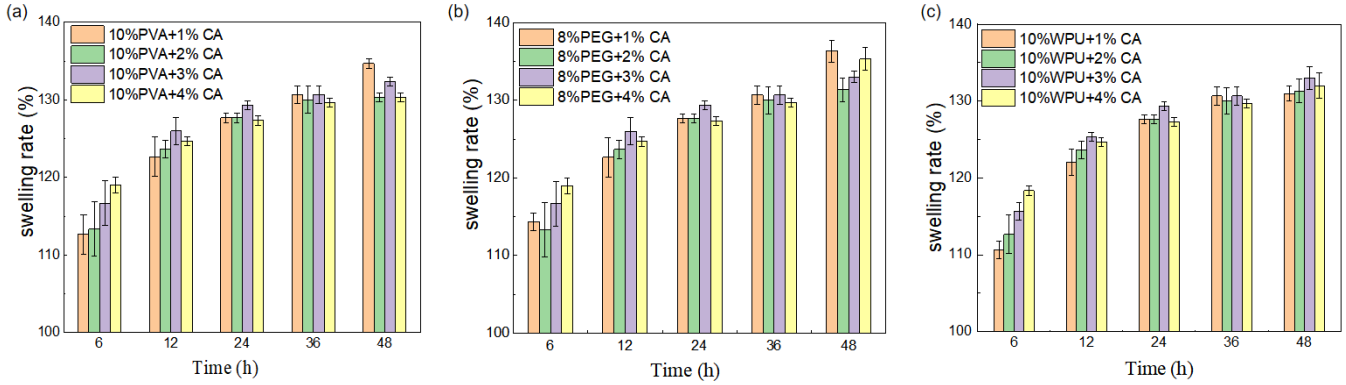

Figure 3. Expansion coefficient of embedded pellets and particles with different embedding materials added to powdered activated carbon: (**a**) PVA; (**b**) PEG; (**c**) WPU.

As shown in Figure 3b, the expansion rates of polyethylene glycol (PEG) and sodium alginate embedded pellets with 1%, 2%, 3%, and 4% activated carbon were 114.8%, 113%, 116%, and 118%, respectively. This order of expansibility is 4%AC > 3%AC > 1%AC > 2%AC. A higher expansion rate could lead to microbial leakage. The 1% activated carbon carrier exhibited stable swelling over 12 h of oscillation, indicating stability in solution. After 48 h, the 2% activated carbon carrier maintained low expansion, ensuring microbial integrity.

As shown in Figure 3c, the swelling performance of water-borne polyurethane (WPU) embedded particles with activated carbon was measured. The addition of activated carbon increased the water absorption and expansion coefficient, improving mass transfer and permeability. The expansion coefficient was more closely correlated with the voidage of the immobilized center. The larger expansion coefficient, well-developed pores, and good permeability facilitated matrix and oxygen entry. The addition of activated carbon enhanced the compactness, service life, and reuse rate of the embedded particles. After 6 h of oscillation, the expansion coefficient increased with activated carbon concentration. After 48 h of shaking, the 1% and 2% activated carbon expansions were similar.

3.1.4. Elasticity Result Analysis

Based on the characterization of the results, we selected three types of embedding balls with different powder activated carbon mass fractions: 2% PVA embedding ball, 2% PEG embedding ball with 3% powdered activated carbon, and 2% WPU embedding particles with 1% powder activated carbon. These were chosen to determine their elasticity. The experimental results are presented in Table 3. The elasticity test involved six types of embedded pellets and particles, revealing that the 2% PVA embedding ball with 2% powdered activated carbon demonstrated the best elasticity.

Table 3. Properties of elasticity.

Number	Immobilized Granules	Elasticity
1	10%PVA-2%SA-2%AC	✔✔✔
2	8%PEG-2%SA-2%AC	✔
3	8%PEG-2%SA-3%AC	✔✔
4	10%WPU-1%AC	✔
5	10%WPU-2%AC	✔✔
6	10%WPU-3%AC	✔

3.1.5. Ammonia Nitrogen Mass Transfer Properties of Embedded Pellets and Particles

The mass transfer resistance of embedded pellets is significantly influenced by the presence of external embedding materials. The mass transfer coefficient (D_e) serves as a more accurate reflection of the mass transfer performance of these pellets and particles. The D_e can be calculated using an equation where the slope k is expressed as $k = \pi^2 D_e / R^2$, and $D_e = k \times R^2 / \Pi^2$. The slope of the embedded carrier is depicted in Figure 4. For the 10% polyvinyl alcohol (PVA)–2% sodium alginate (SA)–2% powdered activated carbon (AC) carrier, the slope was 0.0509. Linear fitting data for the embedded material are shown in Figure 4, and the ammonia nitrogen mass transfer coefficient for the carrier embedded with 10% PVA, 2% SA, and 2% AC was 12.45×10^{-7}. The fitting equations for the PVA (10%), SA (2%), and AC (2%) carrier are $y = 0.0509x + 0.297$, with an R^2 value of 0.98. According to the fitted data, the slope of the embedded pellets is 0.0509. The previous literature suggests that the addition of 2% powdered activated carbon to the embedded pellets enhances their ammonia nitrogen mass transfer coefficient. This is likely due to the activated carbon's larger specific surface area and strong adsorption capacity, which improves the porosity of the carrier and provides numerous adsorption sites. Consequently, the diffusion performance of ammonia nitrogen in the PVA-SA–activated carbon embedded pellets is enhanced.

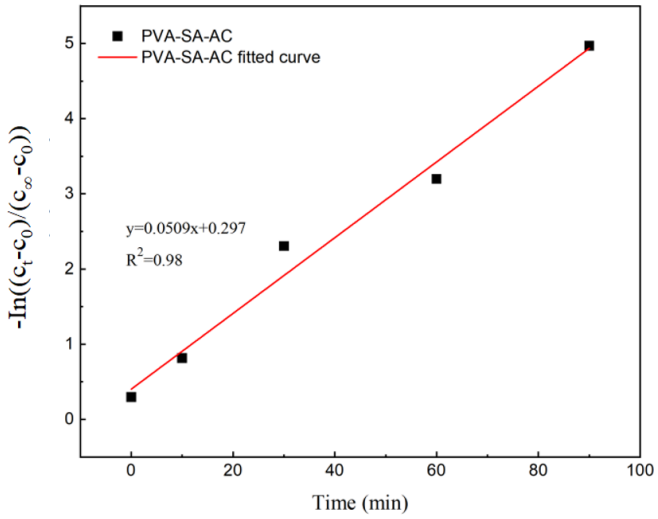

Figure 4. Relationship diagram of cumulative mass transfer performance of ammonia nitrogen afferent inclusion (10% polyvinyl alcohol (PVA)–2% sodium alginate (SA)–2% powdered activated carbon (AC)).

3.2. Batch Experimental Results with Salinity Addition

Figure 5 illustrates that when various concentrations of NaCl are introduced to the influent water, the system's microbial activity temporarily decreases. Specifically, at 15 g/L NaCl, the nitrogen removal efficiency (NRE) is at its lowest, around 40%. This is attributed to the high salinity, which inhibits the activity of the anammox bacteria and their ability to adapt to the high-salt environment. When the salinity exceeds 15 g/L, the osmotic pressure increases, hindering substrate and oxygen transfer and affecting the activity of anammox bacteria (AAOB). At 5 g/L NaCl, the removal rates of ammonia and nitrite nitrogen are higher than at 10 g/L within the initial 6 h. However, after 6 h, the removal rates at 10 g/L are slightly higher than at 5 g/L. This suggests that microorganisms may initially struggle to adapt to the saline environment, leading to activity inhibition.

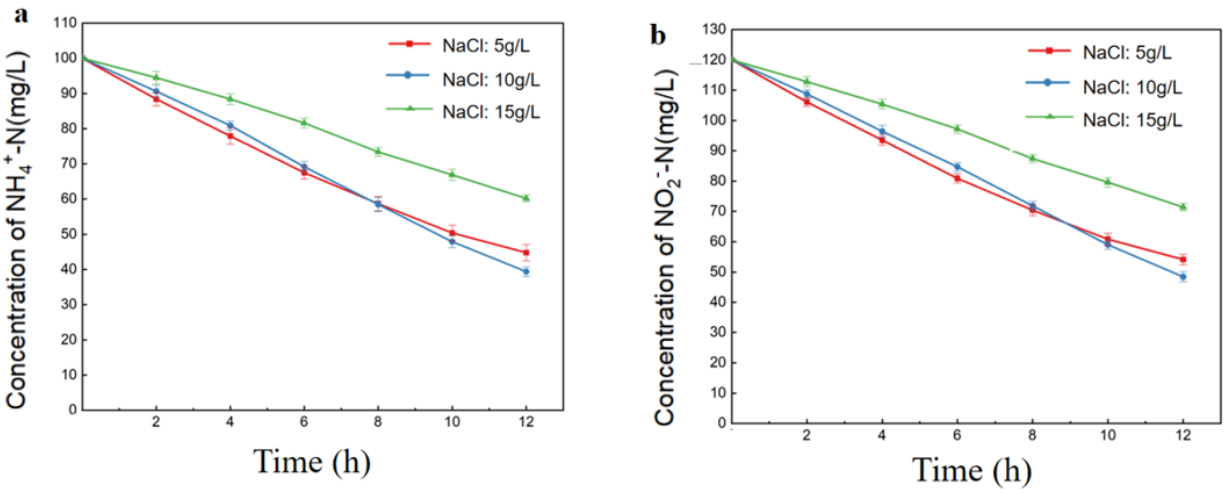

Figure 5. Effects of salinity on anammox pellets: (**a**) ammonia; (**b**) nitrite.

3.3. Performances of Anammox Reactor with Anammox Immobilization Pellets

Throughout the reactor's operation, the concentrations of NH_4^+-N, NO_2^--N and NO_3^--N in the effluent were monitored through daily sampling as shown in Figure 6. The nitrogen load was adjusted based on substrate removal, with the influent concentrations adjusted to manage the nitrogen load. On day one, the influent NH_4^+-N concentration was 100 mg/L, the influent NO_2^--N concentration was 120 mg/L, and the total nitrogen

load of the influents was 0.88 kgN/m^3·d. The concentration of anammox sludge in R_1 was the highest, followed by the concentration of anammox sludge in R_4, R_3 and R_2, which gradually decreased. R_1, with the highest anammox sludge concentration, had the highest NH_4^+-N removal rate of 74.36%. Despite the use of embedded pellets in R_2, R_3, and R_4, their NH_4^+-N removal rates were lower due to the lower sludge concentration before operation. For the unembedded anammox sludge, when the substrate concentration is increased, the NH_4^+-N removal rate will decrease. The NH_4^+-N removal rates of R_1, R_2, R_3 and R_4 were 75.18%, 65.37%, 70.42%, and 72.3%, respectively. From day 3 to day 10, the influent concentrations were gradually increased. R_2, R_3, and R_4 did not see significant changes in removal rate, while R_1's rate increased slightly. This was likely due to the high anammox sludge concentration in R_1, which facilitated rapid anammox reactions and high removal rates. R_1's sludge, predominantly yellowish-brown, still showed some light red areas, indicating anammox activity. The embedded pellets in R_2, R_3, and R_4 transitioned from dark red to light red, with an increase in anammox bacteria content, suggesting improved treatment efficacy at higher substrate concentrations.

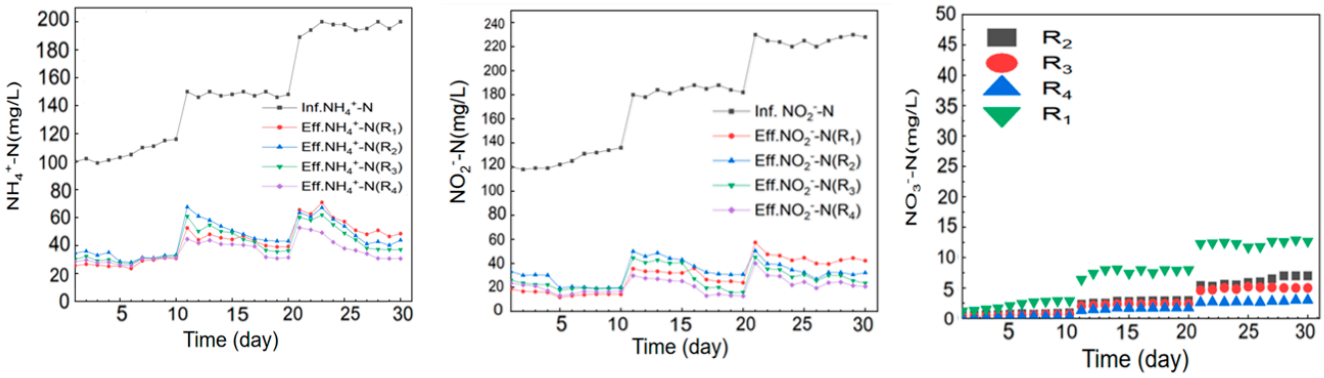

Figure 6. The influent and effluent NH_4^+-N, influent and effluent NO_2^--N, and effluent NO_3^--N.

After day 10, the influent concentrations were increased to 150 mg/L NH_4^+-N and 180 mg/L NO_2^--N. The embedded pellets in R_3 had the highest removal rate, possibly due to their adaptability to environmental changes. R_1's sludge changed from light red to dark red, indicating some inactivation. From day 10 to 20, the concentrations of NH_4^+-N and NO_2^--N in the influent fluctuated at 150 mg/L and 180 mg/L, and the microorganisms in the reactor gradually adapted. R_1, R_2, R_3, and R_4 maintained stable removal rates around 75.5%, 70.89%, 73.5%, and 78.8%, respectively, with a total nitrogen load exceeding 1.1 kgN/m^3·d. The color of the unembedded anammox sludge in the R_1 reactor was yellowish-brown with a reddish color. The color of the embedded pellets in the R_2, R_3 and R_4 reactors gradually changed from light red to dark red. In particular, the embedded pellets in the R_4 reactor are mostly red. The influent substrate concentration was increased again with NH_4^+-N and NO_2^--N concentrations reaching between 200 mg/L and 230 mg/L. Part of the sludge in the R_1 reactor changed from brick red to yellow brown. However, the color transformation of embedded pellets in R_2, R_3 and R_4 reactors was not as obvious as that of the sludge in R_1 reactors. From day 20 to 30, R_3 had the highest NH_4^+-N removal rate, reaching approximately 84.7%.

3.4. Scanning Electron Microscopy Image Analysis

Figure 7 depicts the microstructure of anammox sludge from reactors R_1, R_2, R_3, and R_4 at the 10-day sampling interval. R_1 contained unembedded anammox sludge, while R_2, R_3, and R_4 were inoculated with embedded anammox sludge pellets. The scanning electron microscopy (SEM) images in Figure 7 were taken at ×150, ×1000, ×5000, and ×20,000 magnifications. In the SEM image of the R_1 reactor, granular sludge displayed spherical particles with irregular boundaries, featuring a tight structure and high densification. There was space on the surface of the granular sludge for exhaust gas and material

transportation, and filaments were also observed on the surface for connecting bacteria micelles. Anammox bacteria are closely adhered to and piled together, and mainly exist in the form of a "cluster", which is consistent with the conclusion that anammox bacteria are cluster bacteria. Rod-like and filamentous bacteria were observed, with anammox bacteria closely adhering to each other in clusters, as previously reported.

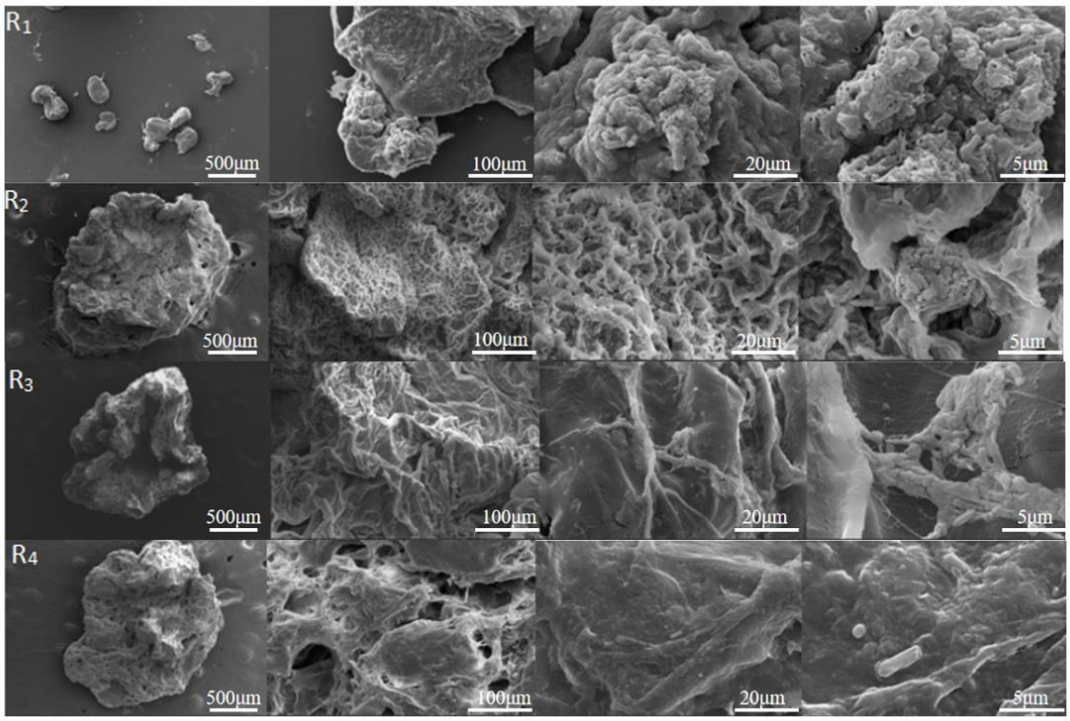

Figure 7. Microstructure of anammox granular sludge and embedded pellets in R_1, R_2, R_3, and R_4 reactors (sampling time 10 d).

The SEM image of R_2 revealed embedded pellets with internal pores, attributed to the addition of activated carbon, which enhances porosity and surface area. Since the embedded material is added with powdered activated carbon, the activated carbon has a porous structure and large specific surface area, the porosity of the embedded particles is improved, and the pores inside the embedded pellets are larger and the number is more, providing enough space for the growth and propagation of anammox bacteria. R_4's SEM image showed irregularly shaped granules, with some being flaky. The dominance of anammox bacteria in this reactor was evident. Anammox granular sludge secretes extracellular polymers (EPs), which contribute to its high retention capacity and facilitate bacterial aggregation. This aggregation results in enhanced growth activity and metabolism, leading to improved nitrogen removal efficiency. Due to the clustering of anammox bacteria, the anammox bacteria gathered together have high growth activity and strong metabolism. The microscopic morphology of anammox sludge underscores its superior microbial retention and high nitrogen removal capability.

4. Conclusions

This research proposed embedding anammox bacteria in a matrix of 10% polyvinyl alcohol (PVA) + 2% sodium alginate (SA) + 2% powdered activated carbon as optimal. These embedded pellets exhibited a settling velocity of 7.43 cm/s, a mechanical strength approaching 97%, an expansion coefficient of 1.32, good elasticity, and a high gel degree. Notably, there was no inter-pellet adhesion observed. The diffusion performance of ammonia nitrogen in embedded pellets is good, and the mass transfer coefficient of ammonia nitrogen can be improved by adding 2% powdered activated carbon. After 30 days of reactor operation, the embedded anammox sludge demonstrated enhanced adaptability to the

external environment, greater resistance to shock loads, and superior removal capabilities compared to granular sludge. Scanning electron microscope analysis revealed that most of the sludge formed irregular granules, with some lamellar structures, signifying the dominance of anammox bacteria in the reactor. In recent years, embedding and immobilization technology has been rapidly developed and widely used, and in the future, it will achieve efficient nitrogen removal in sewage treatment plants.

Author Contributions: Writing—original draft preparation, Y.Y.; writing—review and editing, H.G. and X.D.; methodology, Z.Z. All authors have read and agreed to the published version of the manuscript.

Funding: This research was supported by the Fundamental Research Funds for the Central Universities.

Data Availability Statement: This manuscript is a data-self-contained article, whose results were obtained from the laboratory analysis, and all data are presented within the article.

Conflicts of Interest: The authors declare no conflicts of interest.

References

1. Tuyen, N.V.; Ryu, J.H.; Kim, H.G.; Ahn, D.H. Anammox bacteria immobilization using polyvinyl alcohol/sodium alginate crosslinked with sodium sulfate. *J. Environ. Eng.* **2020**, *146*, 04020020. [CrossRef]
2. Wang, J.; Fan, Y.C.; Chen, Y.P. Nitrogen removal performance and characteristics of gel beads immobilized anammox bacteria under different PVA: SA ratios. *Water Environ. Res.* **2021**, *93*, 1627–1639. [CrossRef] [PubMed]
3. Chen, R.; Ji, J.; Chen, Y.; Takemura, Y.; Liu, Y.; Kubota, K.; Ma, H.; Li, Y.Y. Successful operation performance and syntrophic micro-granule in partial nitritation and anammox reactor treating low-strength ammonia wastewater. *Water Res.* **2019**, *155*, 288–299. [CrossRef] [PubMed]
4. Jenni, S.; Vlaeminck, S.E.; Morgenroth, E.; Udert, K.M. Successful application of nitritation/anammox to wastewater with elevated organic carbon to ammonia ratios. *Water Res.* **2014**, *49*, 316–326. [CrossRef]
5. Laureni, M.; Falas, P.; Robin, O.; Wick, A.; Weissbrodt, D.G.; Nielsen, J.L.; Ternes, T.A.; Morgenroth, E.; Joss, A. Mainstream partial nitritation and anammox: Long-term process stability and effluent quality at low temperatures. *Water Res.* **2016**, *101*, 628–639. [CrossRef] [PubMed]
6. Niu, Q.; He, S.; Zhang, Y.; Ma, H.; Liu, Y.; Li, Y.-Y. Process stability and the recovery control associated with inhibition factors in a UASB-anammox reactor with a long-term operation. *Bioresour. Technol.* **2016**, *203*, 132–141. [CrossRef]
7. Wang, X.; Gao, D. In-situ restoration of one-stage partial nitritation-anammox process deteriorated by nitrate build-up via elevated substrate levels. *Sci. Rep.* **2016**, *6*, 37500. [CrossRef] [PubMed]
8. Bian, W.; Zhang, S.; Zhang, Y.; Li, W.; Kan, R.; Wang, W.; Zheng, Z.; Li, J. Achieving nitritation in a continuous moving bed biofilm reactor at different temperatures through ratio control. *Bioresour. Technol.* **2017**, *226*, 73–79. [CrossRef] [PubMed]
9. Hoekstra, M.; Geilvoet, S.P.; Hendrickx, T.L.G.; Kip, C.S.v.E.T.; Kleerebezem, R.; van Loosdrecht, M.C.M. Towards mainstream anammox: Lessons learned from pilot-scale research at WWTP Dokhaven. *Environ. Technol.* **2018**, *40*, 1721–1733. [CrossRef]
10. Chandran, K.; Smets, B.F. Applicability of two-step models in estimating nitrification kinetics from batch respirograms under different relative dynamics of ammonia and nitrite oxidation. *Biotechnol. Bioeng.* **2000**, *70*, 54–64. [CrossRef]
11. Zhang, D.; Wang, G.P.; Dai, X.H. Operation of pilot-scale nitrification-anammox reactors for the treatment of reject-water produced from the anaerobic digestion of thermal hydrolysis-treated sludge. *Bioresour. Technol.* **2020**, *314*, 127–135. [CrossRef] [PubMed]
12. Munz, M.; Krause, S.; Tecklenburg, C.; Binley, A. Reducing monitoring gaps at the aquifer-river interface by modelling groundwater-surface water exchange flow patterns. *Hydrol. Process.* **2011**, *25*, 3547–3562. [CrossRef]
13. Wett, B.; Hell, M.; Nyhuis, G.; Puempel, T.; Takacs, I.; Murthy, S. Syntrophy of aerobic and anaerobic ammonia oxidisers. *Water Sci. Technol.* **2010**, *61*, 1915–1922. [CrossRef] [PubMed]
14. Lackner, S.; Gilbert, E.M.; Vlaeminck, S.E.; Joss, A.; Horn, H.; van Loosdrecht, M.C. Full-scale partial nitritation/anammox experiences-an application survey. *Water Res.* **2014**, *55*, 292–303. [CrossRef] [PubMed]
15. Piculell, M.; Suarez, C.; Li, C.; Christensson, M.; Persson, F.; Wagner, M.; Hermansson, M.; Jönsson, K.; Welander, T. The inhibitory effects of reject water on nitrifying populations grown at different biofilm thickness. *Water Res.* **2016**, *104*, 292–301. [CrossRef] [PubMed]
16. Jiang, H.; Liu, G.H.; Ma, Y.; Xu, X.; Chen, J.; Yang, Y.; Liu, X.; Wang, H. A pilot-scale study on start-up and stable operation of mainstream partial nitrification-anammox biofilter process based on online pH-DO linkage control. *Chem. Eng. J.* **2018**, *350*, 1035–1042. [CrossRef]
17. Li, X.; Wang, Y.; Li, Y.; Zhou, L.; Jia, X. Biosorption behaviors of biosorbents based on microorganisms immobilized by Ca-alginate for removing lead (II) from aqueous solution. *Biotechnol. Bioprocess Eng.* **2011**, *16*, 808–820. [CrossRef]
18. Schrezenmeir, J.; Kirchgessner, J.; Gerö, L.; Kunz, L.A.; Beyer, J.; Mueller-Klieser, W. Effect of microencapsulation on oxygen distribution in islets organs. *Transplantation* **1994**, *57*, 1308–1314. [CrossRef] [PubMed]

19. Heidebach, T.; Foerst, P.; Kulozik, U. Microencapsulation of probiotic cells for food applications. *Crit. Rev. Food Sci. Nutr.* **2012**, *52*, 291–311. [CrossRef]
20. Olguin, E.J. Dual purpose microalgae-bacteria-based systems that treat wastewater and produce biodiesel and chemical products within a biorefinery. *Biotechnol. Adv.* **2012**, *30*, 1031–1046. [CrossRef]
21. Chávarri, M.; Marañón, I.; Ares, R.; Ibáñez, F.C.; Marzo, F.; del Carmen Villarán, M. Microencapsulation of a probiotic and prebiotic in alginate-chitosan capsules improves survival in simulated gastro-intestinal conditions. *Int. J. Food Microbiol.* **2010**, *142*, 185–189. [CrossRef] [PubMed]
22. Calvet, D.; Wong, J.Y.; Giasson, S. Rheological monitoring of polyacrylamide gelation: Importance of cross-link density and temperature. *Macromolecules* **2004**, *37*, 7762–7771. [CrossRef]
23. Loh, K.C.; Chung, T.S.; Ang, W.F. Immobilized-cell membrane bioreactor for high-strength phenol wastewater. *J. Enviro. Eng.* **2000**, *126*, 75–79. [CrossRef]
24. Rathore, S.; Desai, P.M.; Liew, C.V.; Chan, L.W.; Heng, P.W.S. Microencapsulation of microbial cells. *J. Food Eng.* **2013**, *116*, 369–381. [CrossRef]
25. Mollaei, M.; Abdollahpour, S.; Atashgahi, S.; Abbasi, H.; Masoomi, F.; Rad, I.; Lotfi, A.S.; Zahiri, H.S.; Vali, H.; Noghabi, K.A. Enhanced phenol degradation by *Pseudomonas* sp. SA01: Gaining insight into the novel single and hybrid immobilizations. *J. Hazard. Mater.* **2010**, *175*, 284–292. [CrossRef]
26. Fritzen-Freire, C.B.; Prudencio, E.S.; Amboni RD, M.C.; Pinto, S.S.; Negrão-Murakami, A.N.; Murakami, F.S. Microencapsulation of bifidobacteria by spray drying in the presence of prebiotics. *Food Res. Int.* **2012**, *45*, 306–312. [CrossRef]
27. Pedroso, D.L.; Thomazini, M.; Barrozo Heinemann, R.J.; Favaro-Trindade, C.S. Protection of *Bifidobacterium lactis* and *Lactobacillus acidophilus* by microencapsulation using spray-chilling. *Int. Dairy J.* **2012**, *26*, 127–132. [CrossRef]
28. Cui, J.; Van Koeverden, M.P.; Müllner, M.; Kempe, K.; Caruso, F. Emerging methods for the fabrication of polymer capsules. *Adv. Colloid Interface Sci.* **2014**, *207*, 14–31. [CrossRef] [PubMed]
29. Amigoni, S.; de Givenchy, E.T.; Dufay, M.; Guittard, F. Covalent layer-by-layer assembled superhydrophobic organic-inorganic hybrid films. *Langmuir* **2009**, *25*, 11073–11077. [CrossRef] [PubMed]
30. Liu, T.; Wang, Y.; Zhong, W.; Li, B.; Mequanint, K.; Luo, G.; Xing, M. Biomedical applications of layer-by-layer self assembly for cell encapsulation: Current status and future perspectives. *Adv. Healthc. Mater.* **2019**, *8*, e1800939. [CrossRef]
31. Tanner, P.; Onaca, O.; Balasubramanian, V.; Meier, W.; Palivan, C.G. Enzymatic cascade reactions inside polymeric nanocontainers: A means to combat oxidative stress. *Chem.-A Eur. J.* **2011**, *17*, 4552–4560. [CrossRef] [PubMed]
32. Anselmo, A.C.; McHugh, K.J.; Webster, J.; Langer, R.; Jaklenec, A. Layer-by-layer encapsulation of probiotics for delivery to the microbiome. *Adv. Mater.* **2016**, *28*, 9486. [CrossRef] [PubMed]
33. Yang, S.H.; Kang, S.M.; Lee, K.B.; Chung, T.D.; Lee, H.; Choi, I.S. Mussel-inspired encapsulation and functionalization of individual yeast cells. *J. Am. Chem. Soc.* **2011**, *133*, 2795–2797. [CrossRef] [PubMed]